Proceedings of 31st International Conference on Ocean, Offshore and Arctic Engineering
OMAE 2012
June 10-15, 2012, Rio de Janeiro, Brazil

OMAE 2012-83434

COMPUTATIONAL INVESTIGATION OF IRREGULAR WAVE CANCELATION USING A CYCLOIDAL WAVE ENERGY CONVERTER

Casey P. Fagley

Atargis Energy Corporation
3185 Janitell Road
Colorado Springs, Colorado 80906,
USA
Email: casey.fagley@atargis.com

Jürgen J. Seidel

Atargis Energy Corporation
3185 Janitell Road
Colorado Springs, Colorado 80906,
USA
Email: jurgen.seidel@atargis.com

Stefan G. Siegel*

Atargis Energy Corporation
3185 Janitell Road
Colorado Springs, Colorado 80906,
USA
Email: stefan.siegel@atargis.com

ABSTRACT

The ability of a Cycloidal Wave Energy Converter (CycWEC) to cancel irregular deep ocean waves is investigated in a time integrated, inviscid potential flow simulation. A CycWEC consists of one or more hydrofoils attached eccentrically to a shaft that is aligned parallel to the incoming waves. The entire device is fully submerged in operation. A Bretschneider spectrum with 40 discrete components is used to model an irregular wave environment in the simulations. A sensor placed up-wave of the CycWEC measures the incoming wave height and provides a signal for the wave state estimator, a non-causal Hilbert transformation, to estimate the instantaneous frequency, phase and amplitude of the irregular wave pattern. A linear control scheme which proportionally controls hydrofoil pitch and compensates for phase delays is adopted. Efficiency for the design Bretschneider spectrum shows more than 99% efficiency, while non-optimum, off design operating conditions still maintain more than 85% efficiency. These results are in agreement with concurrent experimental results obtained at a 1:300 scale.

Nomenclature

ε	Efficiency
η	Surface elevation [m]
Γ	Circulation $[m^2/s]$
λ	Wavelength [m]
ω	Frequency [1/s]
Φ	Flow Potential $[m^2/s]$
Ψ	Stream function $[m^2/s]$
ρ	Fluid Density $[kg/m^3]$
Θ	Phase angle [rad]
a	Amplitude [m]
C	Wave Travel Velocity (Celerity) [m/s]
C_g	Wave Group Velocity [m/s]
F	Complex potential $[m^2/s]$
g	=9.81, Gravity constant $[m/s^2]$
H	Wave height
H_s	Significant Wave Height [m]
k	Wave Number [1/m]
P	Power [W]
R	Wave Energy Converter Radius [m]
S	Spectral density $[m^2/(1/s)]$
t	Time [s]
T_s	Standard wave period [s]
u, v	Velocity components [m/s]
W_I	Incoming wave
W_{R-down}	Resulting wave
y_c	Submergence depth [m]
$z = x + iy$	Complex coordinate [m]
$+\lambda_s$	Index denoting down-wave location
$-\lambda_s$	Index denoting up-wave location

*Address all correspondence to this author.

1 Introduction

Among alternative energy sources, wave power is one of the most abundant sources on earth. The World Energy Council according to [1] has estimated the world wide annual amount of wave power energy at 17.5 PWh (Peta Watt hours = $10^{12} kWh$). This amount of power is actually comparable to the annual world wide electric energy consumption, which is currently estimated at 16 PWh. Thus, wave power has the potential to provide a large portion of the worlds electric energy needs, if it can be harnessed efficiently. In addition to the energy availability, wave power has other advantages. Since a large portion of the worlds population lives close to the ocean shores, the distance between energy production and consumption is small, which reduces transmission losses and necessary investments in transmission lines. As opposed to other alternative energy sources like wind, stream and solar energy, the installation of wave power devices does not require use of already precious real estate. Wave energy is also very consistent and predictable providing energy throughout the day and night, but seasonal variations need to be taken into consideration. All of these benefits make wave power an ideal energy source for efficiently providing renewable energy to densely populated coastal areas.

The majority of existing ocean wave energy converters transform the wave energy into reciprocating mechanical motion, which then drives an intermediate power-take-off system that converts the energy to a useful form, with the concomitant efficiency losses in the power take off system. However, it is possible to convert wave energy directly to rotational mechanical energy using a lift based energy converter consisting of one or more rotating hydrofoils aligned parallel with the incident wave crest [2–10]. This wave energy converter is similar to the well established Cycloidal or Voith-Schneider propeller, and is referred to as a Cycloidal Wave Energy Converter (CycWEC). A schematic of the CycWEC, as considered in this paper, is shown in Fig. 1. The CycWEC also has many other fruitful benefits such as maintaining high efficiencies over a range of sea states and standard periods (as shown in this paper), increased survivability by the ability to submerge to safe depths at rough sea states, as well as the possibility of a free floating system. The geometry features two hydrofoils diametrically opposite on a horizontally oriented main shaft at a radius R, rotating clockwise at angular speed ω, and submerged a depth - $y_c > R$. At any point on the free surface the vertical elevation is η and peak-to-peak amplitude of the resulting wave field is H. The incoming ocean wave W_I is assumed to travel left to right, and waves generated by the CycWEC traveling in the direction of the incoming wave are considered traveling in the down-wave direction and are identified as W_{R-down}; while waves traveling in the opposite direction are considered traveling up-wave and are identified as W_{R-up}.

The CycWEC concept was first investigated in the late 1980s by researchers at TU Delft University [8–10]. Experiments conducted at MARIN using a single hydrofoil attached to a submerged horizontal shaft verified that the device could operate as a winch in regular long crested waves. The concept was further investigated both experimentally in [8] and numerically in [10]. This initial work demonstrated the feasibility of the approach, as well as the ability of the CycWEC to self-synchronize with the incoming wave frequency and rotational phase. However, the conversion efficiencies found both in the theoretical work and the wave tunnel experiments were very small, on the order of few percent in experiments, with a theoretical maximum of 15%.

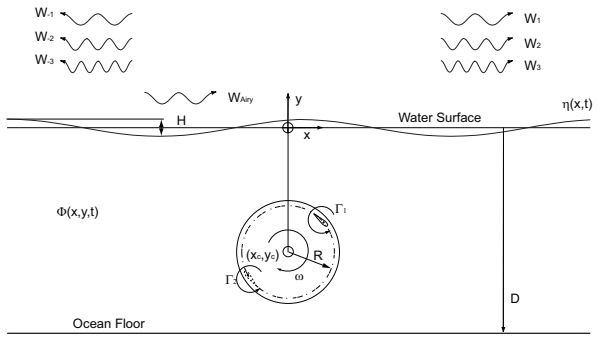

Figure 1. Cycloidal wave energy converter geometry and generated waves

Recent research at the United States Air Force Academy (USAFA) has focused on extending the original work conducted at TU Delft [4]. The primary objective is to increase the device efficiency by operating at significantly higher blade speeds than the wave-induced velocity and by using feedback flow-control to intelligently control the turbine blade orientation and position based on the incident wave field. Initially, computational simulations were performed in [4] and [6] with the device operating as a wave generator with a constant rotational rate and bound circulation. This verified that the CycWEC primarily produces a single-sided wave field and thus is well suited for operation as a wave termination device.

Wave cancelation of both deep and intermediate long crested regular ocean waves was successfully demonstrated in [3, 4] and [6]. Inviscid simulations resulted in device efficiencies in excess of 99%. Wave cancelation experiments at a 1:300 scale have been conducted at USAFA and the results can be found in [4]. Results from the experiments agree well with the computational results in [4] and [6] as $\varepsilon > 90\%$ has been shown for harmonic airy wave fields and $\varepsilon > 80\%$ for irregular wave spectra.

Real ocean waves are random in nature with wave patterns that are ever changing in both time and space. In Jeans et al. [5] numerical feedback simulations showed efficiencies greater than 75% for irregular waves. For irregular wave energy extraction, feedback control is necessary to match the realtime frequency and amplitude of the incoming wave to the CycWEC. The lower efficiency presented in Jeans et al. [5] was not due to the design or performance of the cycloidal wave energy converter but pri-

marily due to suboptimal estimation algorithms which operated the device. This paper focuses on an optimal control strategy which supports more than 99% efficiency for the design operating irregular wave condition as well as above 85% efficiency for off design irregular operating conditions.

2 Computational Model

The CycWEC and wave-induced flow field was modeled using potential flow theory. For an inviscid, incompressible, and irrotational flow, the governing continuity equation simplifies to the Laplace equation,

$$\nabla^2 \Phi = 0 \tag{1}$$

where Φ is the velocity potential. Unique solutions to Equation 1 are determined by satisfying the appropriate boundary conditions based on physical considerations. In seeking two-dimensional solutions it is often convenient to define the complex stream function in terms of the complex coordinate $z = x + iy$,

$$F(z,t) = \Phi + i\Psi \tag{2}$$

where Ψ is the stream function and the complex velocity is defined by $dF/dz = u - iv$.

The simplest representation of a two-dimensional hydrofoil that correctly represents the flow induced in the far field is a point vortex of strength Γ equal to the hydrofoil bound circulation. When the hydrofoil is in the presence of a free surface it is imperative that the appropriate kinematic and dynamic boundary conditions be satisfied on that surface. Derivations of the linearized free surface boundary condition can be found in [11]. Neglecting higher order terms, the kinematic boundary condition ensuring the vertical velocity of the free surface and the fluid are equal is,

$$\frac{\partial \eta}{\partial t} = \frac{\partial \Phi}{\partial y}. \tag{3}$$

The dynamic boundary condition ensuring the pressure on the free surface is atmospheric is determined from Bernoulli's equation. Substituting the free surface elevation for y, and again neglecting higher order terms results in,

$$\eta = -1/g \frac{\partial \Phi}{\partial t}, \tag{4}$$

where $g = 9.81\text{m/s}^2$ is the gravitional constant. Due to the linearization, Equation 4 can be imposed at $y = 0$. A non-reflective boundary condition is applied at the domain boundaries to avoid wave reflections.

Subject to the above boundary conditions, the complex potential for a vortex at $c(t) = x(t) + iy(t)$ in the complex plane moving under a free surface is developed in [12] to be,

$$\begin{aligned} F(z,t) = & \frac{\Gamma(t)}{2\pi i} ln\left(\frac{z - c(t)}{z - \bar{c}(t)}\right) \\ & + \frac{g}{\pi i}\int_0^t \int_0^\infty \frac{\Gamma(\tau)}{\sqrt{gk}} e^{-ik(z-\bar{c}(\tau))} \\ & \times sin\left[\sqrt{gk}(t-\tau)\right] dk d\tau \end{aligned} \tag{5}$$

where $\Gamma(t)$ is the circulation of the vortex, and k the wave number. It is important to note that in Equation 5 the fluid is assumed to be infinitely deep.

Each CycWEC hydrofoil is modeled by numerically integrating Equation 5 using a second order time and wave number marching technique. To ensure that the numerical solution converges, numerical integration settings for Δt, Δk, and k_{max} were chosen based on the results of the convergence study presented in [4]. Equation 4 is then used to determine the resulting surface elevation and wave pattern. The theory of superposition is used to extend this approach to a CycWEC with two hydrofoils, where the total potential is determined from $\Phi_{total} = \sum_{i=1}^{2} \Phi_i$ and Φ_i is the potential of each hydrofoil.

The hydrofoil bound circulation $\Gamma(t)$ is a function of the instantaneous wave height and is determined from the implemented feedback flow-control scheme. It should be noted that no wake model is implemented to ensure that Kelvin's conditions is satisfied at each time step. In actuality each hydrofoil would shed vorticity into its wake of an amount equal to the change in bound circulation. Thin hydrofoil simulations presented in [4] showed that this effect is negligible for far field estimates of surface elevation when the hydrofoil chord is small relative to the wave length.

2.1 Irregular Wave Model

The irregular incident wave field is modeled using a linear superposition of a finite number of linear Airy wave components. The fidelity of the irregular wave field will increase as the number of wave components is increased. According to [13], a minimum of 20 wave components are required for modeling a unidirectional irregular seaway. The amplitude for component i is based on a specified wave spectrum according to,

$$a_i = \frac{H_i}{2} = \sqrt{2 S_I(\omega_i)\Delta\omega_i}, \tag{6}$$

where S_I is the spectral density and $\Delta\omega_i$ is the wave frequency interval for component i.

For the current study the incident wave field is modeled using the Bretschneider wave spectrum, which is a commonly used two parameter model for wave spectra in the open ocean. The Bretschneider spectrum is defined as [14],

$$S_I(\omega) = \frac{486.0 H_s^2}{T_s^4 \omega^5} \exp \frac{-1948.2}{T_s^4 \omega^4}, \tag{7}$$

where H_s is the significant wave height and T_s is the wave period associated with the peak energy. The Bretschneider wave spectrum is non-dimensionalized by the standard wavelength λ_s and the standard period T_s as shown in Fig. 2. Also shown are the resulting wave components when the spectrum is divided into 40 wave components with $0.7\omega_s \leq \omega \leq 1.3\omega_s$. With the period and amplitude of each component wave defined, the associated wave length and power can be determined from Airy wave theory. The wave length is determined from the dispersion relationship as follows,

$$\lambda_i = \frac{T_i^2 g}{2\pi}, \tag{8}$$

where λ_i and T_i are the wavelength and period of component i. The wave power per unit length, P_i, associated with each component is related to the wave height and period by,

$$P_i = \frac{1}{32\pi} \rho g^2 H_i^2 T_i. \tag{9}$$

Since the wave power scales linearly with the wave period, higher harmonic waves of the same wave height will contain less energy in proportion to their period. Also note the quadratic relationship between wave energy and wave height. A typical time history of the resulting wave surface is shown in Fig. 3. This is formulated by the linear combination of each component with random phase between $\theta = 0$ and $\theta = 2\pi$.

2.2 Feedback Flow Control Model

For the successful cancelation of an unknown, incoming airy wave, feedback control and wave state estimation are necessary for operation of the CycWEC. Algorithms to interpret and estimate the wave state in real time fashion are needed to adequately control and efficiently extract energy. The wave state for a single Airy wave is defined as its phase θ, frequency ω, and wave height H. A sensor which measures the surface elevation over time is placed upstream of the CycWEC. This measurement is defined as $\eta(t)$ and for a single Airy wave displays a purely periodic signal with unknown frequency and amplitude. The implemented feedback control scheme is shown in Figure 4. The sensor relays

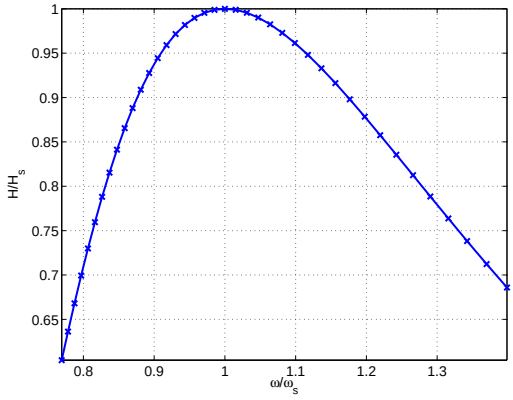

Figure 2. Bretschneider spectrum discretized into 40 components over the range of $0.7\omega_s \leq \omega \leq 1.3\omega_s$

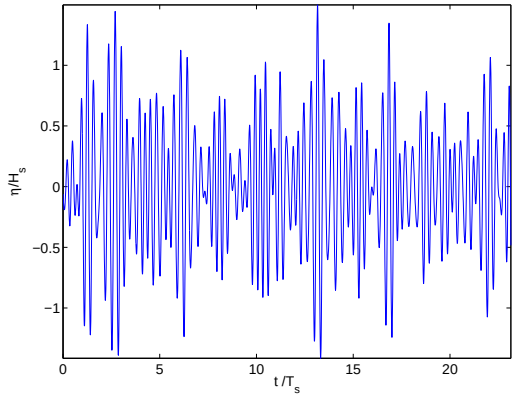

Figure 3. Time history of 40 component Bretschneider wave linearly superimposed with randomized phase

a signal to the estimator which estimates the wave height, phase and period. The controller then computes the rotational position and blade angle to generate an opposing wave that effectively cancel the incident wave field.

Given a time history of the upstream measurement, a relation is sought such that $[\hat{\omega}(t)\hat{\phi}(t)\hat{H}(t)]^T = f([\eta(t), \eta(t-1), \ldots, \eta(t-n)]) + e(t)$ with minimal estimation error, $e(t)$. A typical Fourier analysis falls short because instantaneous phase information is lost in the decomposition. Therefore, other digital signal processing methods need to be implemented. Because the up-wave wave height measurement contains no negative frequency components, the signal can be expressed as an analytic signal such that,

$$\eta(t) = \frac{1}{2\pi} \int_0^\infty \eta(\omega) e^{i\omega t} d\omega. \tag{10}$$

A complex representation of a periodic signal is $e^{i\omega t} =$

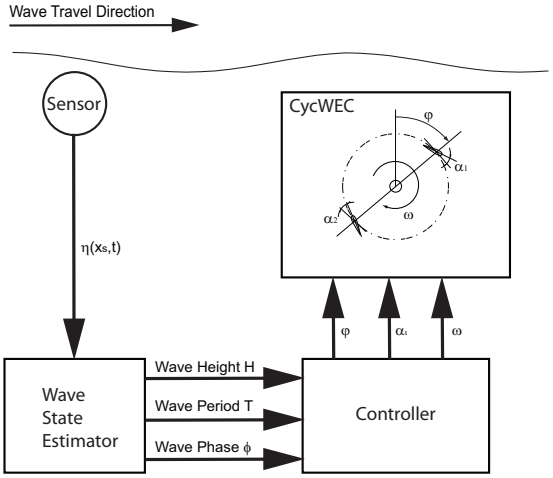

Figure 4. Block diagram of the implemented feedback flow control scheme for the cycloidal wave energy converter.

$\eta(t) + i\hat{\eta}(t)$. The complex component of the analytic signal, which is unknown at this point, is analogous to the Hilbert transformation, $\mathcal{H}[\bullet]$, of the real component; that is $\hat{\eta}(t) = \mathcal{H}[\eta(t)]$. The Hilbert transformation is a linear filter which produces a phase shift of $\pm\frac{\pi}{2}$ over all frequencies present in the signal, $\eta(t)$. In the time domain the transformation for this linear filter is identically the convolution with $\frac{1}{\pi t}$ which is shown as,

$$\mathcal{H}[\eta(t)] = \frac{1}{\pi t} * \eta(t) = \frac{1}{\pi}\int_{-\infty}^{\infty} \frac{\eta(t-\tau)}{\tau} d\tau. \tag{11}$$

In the frequency domain the transform of the signal $f = \frac{1}{\pi t}$ is

$$-isgn(f) = \begin{cases} -if > 0 \\ 0 f = 0 \\ if < 0 \end{cases} \tag{12}$$

The transfer function of this ideal filter will have a magnitude of one and phase of $\pm\frac{\pi}{2}$ for $\pm\omega$, respectively. Because the Fourier transform is a non-causal transformation (dependent on previous, current and future measurements), an approximation to this transformation is necessary. Typical filters such as finite impulse response (FIR) and infinite impulse response (IIR) filters can be designed to simulate the response of $\frac{1}{\pi t}$. As for the purposes of this paper a 3 stage cascading IIR filter is used to estimate the complex component of the Hilbert transformation with minimal phase (although non-linear) delays at the designed frequency.

Now that the real and complex components of the analytic signal are known to some degree of error, the instantaneous amplitude is estimated from the L_2 norm of the signals, (i.e., $\hat{H}(t) = \|\eta(t) + \hat{\eta}(t)\|_2$). The instantaneous phase is then computed as the angle between the real and complex estimate as, $\hat{\phi}(t) = \arctan(\frac{\hat{\eta}(t)}{\eta(t)})$. The instantaneous frequency is the time derivative of the phase estimate.

As seen in Fig. 4, the wave state is now fully estimated. The control scheme is very basic for the purposes of this paper. Proportional control is used for the blade pitch (i.e., bound circulation), such that $\alpha_i(t) = P_{gain}\hat{H}(t)$. This is a reasonable assumption as open loop wave generation results shown in [4] display a very linear relationship between the bound circulation and resulting wave height. As for rotary control of the propeller the group velocity is estimated and compensated for as a phase delay. The time delays are then superimposed to control the rotational velocity of the main shaft in a stepwise fashion, such that $\theta(t) = \hat{\phi}(t) + \frac{\eta_{\lambda_s}}{C_g} + \theta_f$, where C_g is the group velocity of the wave, θ_f is the phase compensation of the Hilbert transformation filter, η_{λ_s} is the measured surface elevation at a distance of λ_s in the up-wave direction, and $\hat{\phi}(t)$ is the estimate of the real time phase.

3 Results and Discussion

To analyze the performance of the CycWEC over a range of varying wave irregular states, sea state probability data tabulated in the Northern Atlantic was taken from [14]. The data gave the statistical probability of the occurrence of a particular sea state in terms of standard period and significant wave height. The data is presented in number of hours in which that sea state occurred throughout the year. Because the power varies linearly with wave period and quadratically with significant wave height, the data was modified by a weighting matrix to estimate the power at each sea state. The resulting power scatter plot is presented in Fig. 5. The scatter diagram is normalized ($T/T_s = 1$) to the peak power location which is the design point for the CycWEC; that is as further described in [3] the optimum radius of the CycWEC is

$$R = \frac{\lambda}{2\pi} = \frac{gT_s^2}{(2\pi)^2}. \tag{13}$$

The simulation parameter space was designed to span the range of the scatter plot shown in Fig 5. The parameter varied was the radius of the CycWEC. The radius ranged from $\frac{2R}{\lambda} = 0.1 \rightarrow 1$ with a total of 17 simulations performed over that range. Each simulation used discretization parameters (temporal and wave number) as presented in previous publications [3]. Each simulation was performed such that feedback control was started at $t = 2s$ and continued throughout the remainder of the simulation. Typical resulting wave patterns are shown in Figure 6 at the up-wave ($x = -1\lambda$) and down-wave ($x = +1\lambda$) directions. The case presented in Figure 6 is the optimal design case at which $2\pi R = \lambda$. As shown, the down-wave wave height is significantly reduced by the CycWEC indicating that the majority of the energy has been extracted.

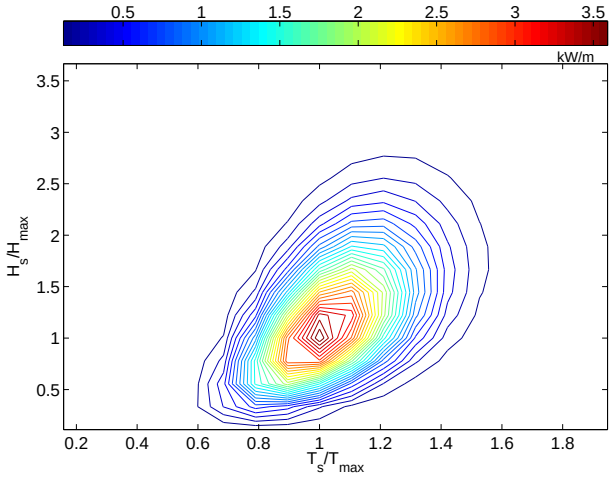

Figure 5. North Atlantic scatter diagram normalized to CycWEC design period of $T_s = 1$. Data is represented in $Watt - hr/mwavecrest$.

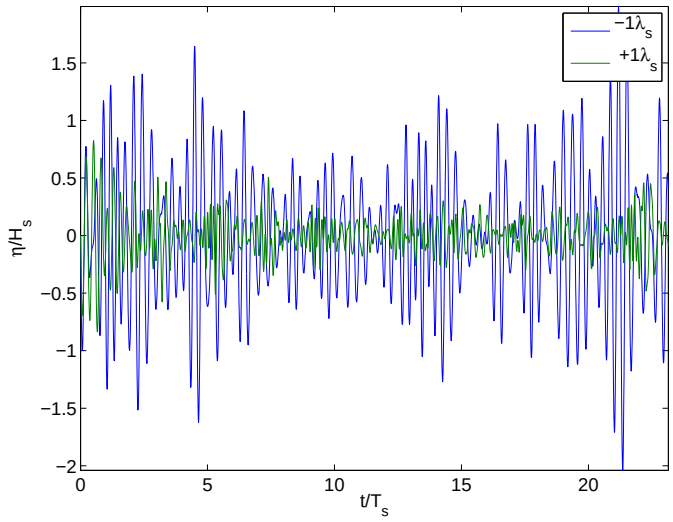

Figure 6. Surface elevation at up-wave (-1λ) and down-wave ($+1\lambda$) locations for case $R = \lambda/2\pi$

The entire surface was computed for the simulation of the design case for the spatial range of $-1 \leq x/\lambda \leq 1$. The space-time plot is shown in Figure 7 for only a time segment of the simulation. It can be seen that the wave height is reduced spatially as well as temporally.

The primary figure of merit for the CycWEC design is the percentage of the wave energy extracted from the incident wave field, defined as the device hydrodynamic efficiency, ε. The efficiency is determined from a control volume analysis based on

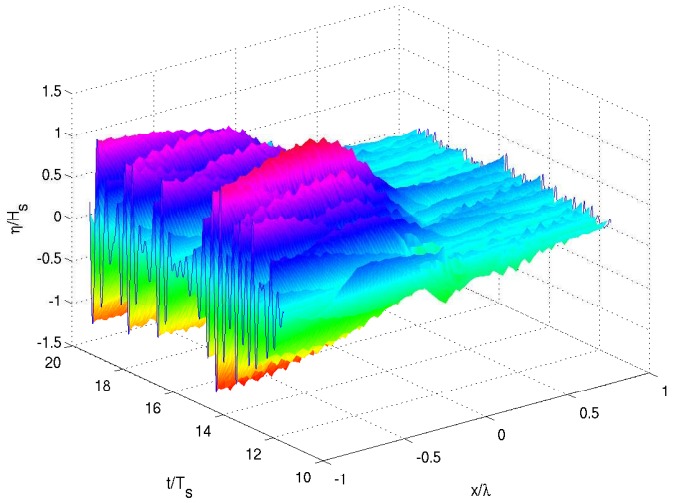

Figure 7. Surface elevation as a function of time and space. Unidirectional airy waves travel in the $+x$ direction. The CycWEC is located at at the $x = 0$ position and terminates all waves in the $+x$ direction.

energy conservation which is implicit in the unsteady Bernoulli equation. The analysis assumes that all energy leaving or entering at the up–wave and down–wave boundaries is contained in traveling Airy type waves. Thus, the power difference at both boundaries is to be provided or absorbed by the CycWEC hydrofoils. The domain boundaries are located at $\pm\lambda$. The hydrodynamic efficiency is defined as,

$$\varepsilon = 1 - \frac{P_{-\lambda}}{P_{+\lambda}}, \tag{14}$$

where the power is computed from Equation 9. The hydrodynamic efficiency will reach a value of one when the incident wave field at the upwave boundary is undisturbed by the CycWEC and the wave field at the down-wave boundary approaches zero.

The resulting wave fields at the up- and down-wave boundaries (i.e., $x = \pm\lambda$) are analyzed using a fast Fourier transform. To ensure that initial transients did not affect the analysis transformation, data prior to $t = 5s$ was discarded. To determine the total power in the wave fields P_{R-up} and P_{R-down}, each wave component identified in the FFT was assumed to be an Airy type and its associated power was determined from Equation 9. The resulting hydrodynamic efficiency was then determined using Equation 14.

The resulting spectra of wave height and wave power after an FFT analysis are shown in Figure 8 a) and b), respectively. The computed efficiency for this optimal case was $\varepsilon = 99.45\%$. The control output/CycWEC inputs are shown in Figure 9. As

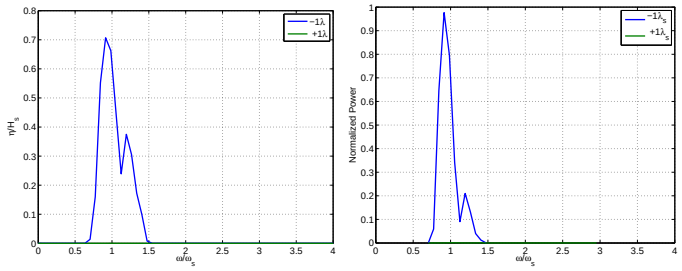

(a) (b)

Figure 8. Fourier analysis of resulting wave surface a) height b) power for the design case. Efficiency for this simulation is $\varepsilon = 99.45\%$

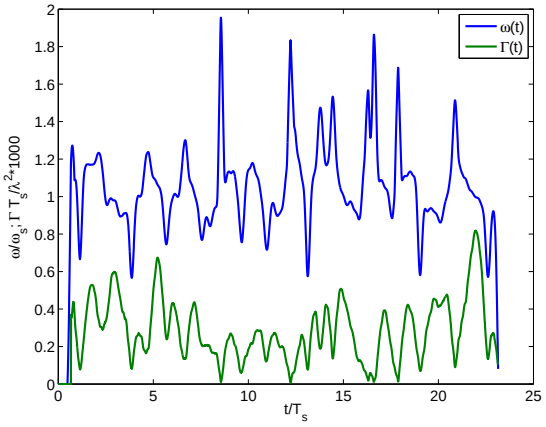

Figure 9. Controller output for near optimal design case, $R = \lambda/2\pi$.

seen the controller output is highly irregular in both frequency and bound circulation, but feedback is essential for energy extraction in an unknown wave field. This same approach was carried out for the entire parameter range and is summarized by the efficiency of energy extraction based on the approach presented in Equation 14. The summary of the overall irregular efficiencies is plotted in Figure 10 in blue. As shown the efficiency remains near 100% for a large portion of the off design operating ranges. This compares very nicely with harmonic wave cancelation efficiencies also plotted in Figure 10 in green which was published in [3]. As expected the reduction in efficiency does occur sooner within an irregular wave environment as the device becomes further off design when compared to the harmonic results. It is important to note that as the WEC becomes small in comparison to the standard wave length ($2R/\lambda_s < 1/\pi$) the efficiency begins to trail off at a quicker rate than in the opposite situation ($2R/\lambda_s > 1/\pi$).

To evaluate the yearly efficiency the performance of the CycWEC is analyzed over a yearly likelihood of wave period variations. The North Atlantic scatter data which is plotted in Figure 5 (data from [14]), provides a means to compute the annual wave energy for this North Atlantic location. This is plotted in Figure 10 as the red curve. The radius of the WEC is then designed for this sea location to maximize the yearly output efficiency. For this situation the radius of the WEC is designed similar to the previous optimal relationship, $2R/\lambda = 1/\pi$, to fully encompass the range of variation in the wave periods recorded at that location. Next, an estimate of the yearly efficiency is computed from Equation 14, where the energy lost (i.e., energy not converted to electricity) is also plotted in Figure 10 in cyan. Finally, those two curves are integrated and an estimate of the yearly efficiency is computed as $\varepsilon_{annual} = 98.3\%$.

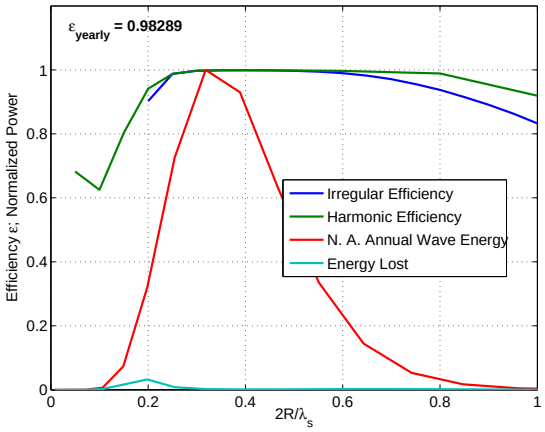

Figure 10. Overall efficiency performance vs. WEC size to wavelength ratio for harmonic and irregular airy waves. An optimally designed WEC in which $2\pi R = \lambda_s$ as in [3] shows yearly efficiency of 98.3% in a North Atlantic sea state probability.

4 Conclusion

Simulations results of wave cancelation in irregular, unidirectional deep ocean waves using a Cycloidal wave energy converter (CycWEC) are presented. The simulation which has been experimentally validated at the 1:300 scale is a time integrated, inviscid potential flow solution subject to a linearized free surface boundary condition. Wave irregularity is modeled by the commonly accepted Bretschneider spectrum discretized by 40 components. The irregular spectrum is varied over a range of standard periods (T_s) to represent corresponding sea state variations in a North Atlantic environment. A non-causal Hilbert transformation of the up-wave surface elevation is used to accurately and efficiently estimate the instantaneous frequency, phase and amplitude of the irregular wave surface. A proportional control scheme is adopted to control blade pitch of the CycWEC. Phase compensation is also necessary to model the group velocity of the irregular wave packets between the up-wave sensor location and the CycWEC. Efficiencies are computed from a control volume analysis by up and down-wave surface elevations.

The efficiency of the CycWEC is shown to be above 85% for the entire range of standard wave periods and above 99% for the optimal design case. The CycWEC efficiency in irregular wave climates aligns very nicely with previously published harmonic efficiency analysis. Annual estimates of efficiency were computed from North Atlantic sea likelihood data and showed that 98.85% of the energy was extracted over the course of a year. These results show that the CycWEC is truly a wave termination device over a large band of irregular waves. In a companion paper, OMAE 2012-83388, the irregular wave cancelation results are verified experimentally.

Future work on the CycWEC is to extend the current simulations to incorporate an estimate of shaft torque as well as viscous losses. As for the experiments, a 1:10 scale device is currently being designed and setup and will be tested in 2012.

ACKNOWLEDGMENT

The authors would like to acknowledge fruitful discussion with Dr. Tiger Jeans. This material is based upon work supported by the Department of Energy under Award Number DE-EE0003635.

Disclaimer

REFERENCES

[1] Boyle, G., 2004. *Renewable Energy - Power for a sustainable future*. Oxford University Press.

[2] Siegel, S., Jeans, T., and McLaughlin, T., 2009. "Deep ocean wave cancellation using a cycloidal turbine". In 62nd Annual Meeting of the American Physical Society, Division of Fluid Dynamics, Minneapolis, MN.

[3] Siegel, S. G., Jeans, T., and McLaughlin, T., April 2011. "Deep ocean wave energy conversion using a cycloidal turbine". *Applied Ocean Research,* ***Volume 33 Issue 2***, pp. 110–119.

[4] Siegel, S., Roemer, M., Imamura, J., Fagley, C., and Mclaughlin, T., 2011. "Experimental wave generation and cancellation with a cycloidal wave energy converter". In 30th International Conference on Ocean, Offshore and Arctic Engineering (OMAE), no. OMAE2011-49212.

[5] Jeans, T., Siegel, S. G., Fagley, C., and Seidel, J., 2011. "Irregular deep ocean wave energy conversion using a cycloidal wave energy converter". In 9th European Wave and Tidal Energy Conference (EWTEC),Southampton, UK, September 5th 9th.

[6] Siegel, S. G., and McLaughlin, T., 2010. "Ocean wave energy conversion using a cycloidal wave energy converter". In 4th Alternative Energy NOW Conference, Lake Buena Vista, FL.

[7] Pinkster, J., and A.J.Hermans, 2007. "A rotating wing for the generation of energy from waves". In 22nd IWWWFB Conference, Plitvice, Croatia.

[8] Marburg, C., 1994. "Investigation on a Rotating Foil for Wave Energy Conversion". Master's thesis, TU Delft.

[9] Hermans, A. J., van Sabben, E., and Pinkster, J., 1990. "A device to extract energy from water waves". *Applied Ocean Research Computational Mechanics Publications,* ***Vol. 12, No. 4***, p. 5.

[10] van Sabben, E., 1987. "De in het snelheidsveld van lopende golven ronddraaiende plaat; invloed op het vrije vloeistofoppervlak". Master's thesis, TU Delft.

[11] Newman, J. N., 1977. *Marine Hydrodynamics*. MIT Press.

[12] Wehausen, J., and Laitone, E., 1960. *Surface Waves, Handbook of Physics, Vol.9*. Springer-Verlag.

[13] McTaggart, K., September 2003. Modelling and simulation of seaways in deep water for simulation of ship motions. Tech. Rep. Tech. Rep. DRDC Atlantic TM 2003-190, Defence R&D Canada - Atlantic.

[14] IACS, 2000. No 34. standard wave data. Tech. rep., International Association of Classification Societies LTD.